Short-term HRV using acceleration PPG under severe ambient settings using in-house developed wearable

Payal Mohapatra[1] and Preejith S P[2] and Mohansankar Sivaprakasam[1,2]

***Abstract*— The utility of heart rate variability (HRV) in clinical diagnosis, treatment of cardiovascular diseases, metric for social and mental well-being and physical fitness, is paramount. The gold-standard is to extract the variability information from the RR-intervals in ECG. Use of PPG as a surrogate to ECG have been put forth recently by many studies. In the presented work the use of wrist based PPG as an alternate to ECG for HRV is proposed. This would help in expanding the serviceability of wearable and portable heart rate monitors or simplify ambulatory monitoring of HRV. A novel optical sensor utilising yellow−orange emitters is designed to pick up optimal PPG signal from the dorsal side of the wrist using reflective plethysmography technique under no significant motion. The second-derivative approach is chosen to identify pulse intervals from PPG. The sensor and algorithm are validated on 5 subjects in particularly low temperature and high altitude conditions of Ladakh. Inspite of the potential setback due to the ambient conditions, on PPG acquired from the wrist, the optical sensor could pick up very good quality signals. The algorithm is also highly sensitive. Also the derived features and the intervals obtained from wrist-PPG are within a confidence of 5 % from that of ECG derived parameters.**

I. INTRODUCTION

The cardiac cycles of a healthy human heart are not constant. This variation in the subsequent cardiac cycles is referred to Heart Rate Variability (HRV). The manifestation of the Autonomic Nervous System's (ANS) sympathetic and parasympathetic pathways in HRV, makes it an ideal choice for non-invasive detection of many cardiological risks [1], physical training [2], psychological well being [3] etc. Altogether HRV analysis holds significance in the assessment of psychic and somatic fitness. Studies have highlighted the diagnostic value of short-term HRV (5-minute)[4]. Agreement between the time-domain features of HRV derived from short term recordings with those of the long-term analyses have been presented in [5].

Owing to the simplicity of the operation of photoplethysmography (PPG), wide applicability in clinical routine [6] and increasing incorporation in wearable health monitoring devices, it is desirable to explore additional measurements which can be derived from PPG. There are studies which prove the surrogacy of HRV derived from the variation of inter-pulse intervals in PPG to the HRV derived from the gold-standard ECG [7]. Most the studies performed to show the agreement of PPG to derive HRV with ECG have used only the extremities of the body as the measurement site of PPG such as finger, earlobes [8] etc.

The presented work justify the use of wrist based PPG placed at the dorsal side of the arm as a compliable method to derive the time domain features of short-term HRV under adverse climatic conditions. Agreement of the extracted pulse interval variation to that obtained from an ECG have also been illustrated. All the derived features of HRV used in the proposed system adhere to the standards specified by [9]. The distinctive feature of wrist being the measurement site is, its non-peripheral location which harbors lower perfusion levels than that of the extremeties of body . Also sensor placement on the dorsal side of wrist is used to measure the PPG, since this is the preferred location of most wearable health monitors using PPG technique over the ventral side. To obtain HRV parameters within the agreeable limits from wrist PPG, a novel optical sensor design is proposed which maximises the signal quality and a second-derivative approach is implemented on the PPG signals to evaluate the pulse intervals. High altitude, lower oxygen levels and temperature affect the human autonomic system's response and hence the HRV [10]. This study is an attempt to validate the agreement of our developed sensor in conjunction with the algorithm to provide HRV features in such adverse climatic adaption and acclimatization.

II. STUDY OBJECTIVE AND DATA COLLECTION

The goal of this study is to investigate the use of wrist based PPG to analyse time-domain features of short-term HRV. To aid this objective, data are collected from 5 healthy subjects with an age distribution of 31 ± 3 in two locations (Leh and Pankong Lake) of Ladakh. The average temperature during the data collection period was 6°C, oxygen levels varied between 82%-92% at an altitude of 3400 meters. Such low levels of atmospheric temperature increase superficial microcirculation and hence a potential deteriorating factor in the signal quality of the acquired wrist based PPG. The subjects had undergone appropriate acclimatization prior to data acquisition. The subjects were explained the protocol of measurement and familiarised with the equipment before starting the data collection. Biocompatible ECG electrodes were used to collect the ECG signals in single lead configuration. The developed PPG sensor is secured snugly around the subject's wrist. The subject is confirmed for any case of discomfort. The PPG and ECG data are simultaneously recorded for a period of five minutes in pelvic upright sitting posture.

[1]Department of Electrical Engineering, Indian Institute of Technology Madras, Chennai-600036, India (Currently working as an employee with Analog Devices Inc., Bangalore, 560093) mohapatrapayal01@gmail.com

[2]Healthcare Technology Innovation Centre Indian Institute of Technology Madras, Chennai-600113, India

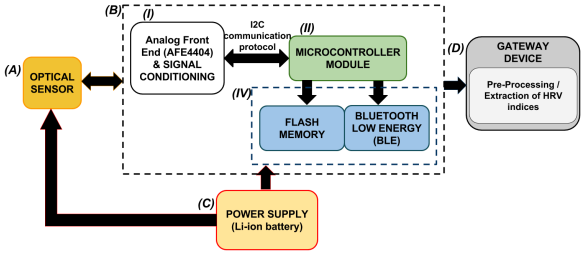

Fig. 1. System level architecture. The modules are labeled as (A) optical sensor unit, (B) mother board consisting of (I) system hardware (analog front end and signal conditioning circuit, digital accelerometer), (II) microcontroller unit, (III) data storage and streaming unit, (C) power unit and (D) gateway device (tablet/personal computer/smart-phone).

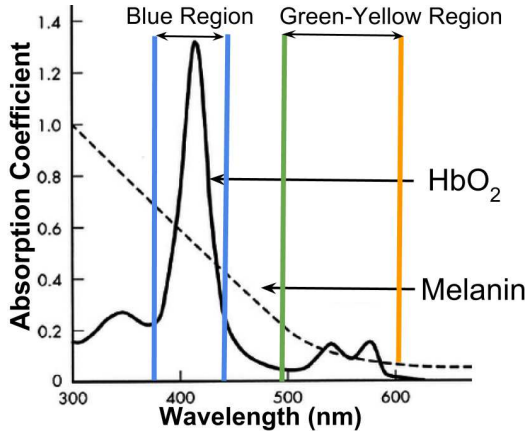

Fig. 2. Relation between melanin and HbO_2 absorption coefficient and wavelength [30].There is a progressive decrease in melanin absorption coefficient with increase in wavelength. Hence, the choice of wavelength with escalated HbO_2 absorption is made towards the secondary peak ranging between 500 nm - 600 nm to have relatively less sensitivity to melanin.

III. MEASUREMENT METHODOLOGY

A wrist-based optical wearable is designed using the technique of reflective photoplethysmography, to work in conjunction with a host processor. A yellow-orange (590 nm) wavelength optical sensor topology is used, which is relatively insensitive to skin pigmentation levels [11]. Further details supporting this choice is given in Section III-A. The motherboard houses an analog front end, AFE4404 by Texas Instruments, a microcontroller unit to program the basic functionalities and communication between the modules, and a data streaming and storage unit for off-line data analysis. The modular level break-down is shown in the system architecture in Fig. 1 with detailed annotations. This system is capable of measuring HRV indices (time and frequency) with a high degree of confidence (α<5%). The algorithms for pre-processing and extraction of HRV indices are employed in the host processor for either off-line or real-time analyses, as required.

A. Optical Sensor Design

In reflective PPG, optical emitter unit is used to shine light onto the measurement site, whose properties are modulated by the direct pulsation in arteries or palpated through the capillaries. This pulsatile quasi-periodic optical signal is received by a photodetector. The bones, tendons, muscles, fat etc. introduce an additional time-invariant component to the acquired signal. Quality of signal picked up by the sensor largely depends on the optical properties of skin as well. Anderson and Parrish have reported an absorption window of 350 nm - 1200 nm for melanin [12]. Such a dermal property hinders the strength of signal picked up by the photodetector for pigmented subjects. From Fig. 2 a decrease in the absorption coefficient of melanin with progressing wavelength can be seen. Since, water absorbs light with wavelength greater than 1000 nm , wavelengths beyond 1000 nm are not suitable as optical emitters. Superiority of shorter wavelengths like green over IR have been shown in literature [13]. Infra-Red (IR) light has a high optical penetration depth [14]. This makes IR extremely susceptible to even mild movements, hence, less suitable for wrist-based wearables. Hence, the identification of suitable wavelength for the current optical emitter was conducted in the visible spectrum. From Fig. 2, it can be observed that the dominant peak of the HbO_2 absorption coefficient is in blue-region, followed by yellow-green region. Since, melanin absorption coefficient is high in the blue-region the signal quality was found to be poor. Further tests were conducted in the green-yellow region, between 500 nm-600 nm to identify the wavelength which provides the strongest signal corresponding to pulsatile blood flow. Experiments were conducted on numerous LEDs with wavelengths in the range of 500 nm-600 nm subject to their commercial availability, and the results attained with 590 nm (yellow-orange) wavelength were the most favorable. This is a justified choice, as towards the later end of the span of chosen visible-spectra, there is prominently high absorption coefficient for HbO_2 and relatively lower absorption corresponding to melanin. A study on the response of 590 nm wavelength as compared to the traditional choice of green (500 nm-540 nm) wavelength on varied skin-tone subjects is presented and affirmative results on the relative insensitivity of 590 nm optical scheme to melanin is reported in the previous work of the authors [11]. Such a choice allows to expand the utility of the wearable to subjects with varied skin pigmentation levels.

The proposed design for optical sensor configuration has two fundamental units: emitter and detector. A wide band photodiode (PD) (TEMD5080X01) with an exposed area of reception of 70 mm^2 and a comparable spectral response over the entire visible region is used in the as the detector in the design. Black package dome lens (beam angle of 30°) light emitting diodes (LED) are used as the optical emitters. The 30° beam angle ensures enhanced focus and intensity. The black package reduces reflections caused by incident light or any other light bleeding issues. A 590 nm (yellow-orange) LED (LYT64F) is used in the design.

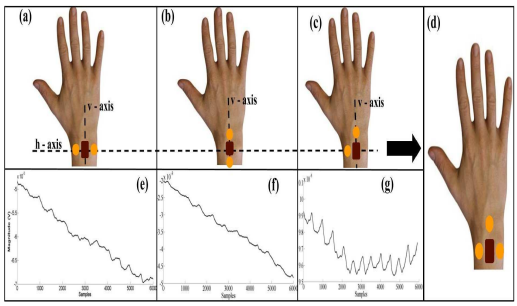

Fig. 3. Experimentation with different optical topologies.(a,b) LEDs placed at 180° with respect to each other. (c) LEDs placed at 90° with respect to each other with the vertex at the photodiode. (d) Final topology with a symmetrically opposite LED along the h-axis to provide redundancy in case of loss of contact in the event of tilt or improper placement by wrist bone.(e-f) Waveforms corresponding to configurations shown in (a-c) respectively.

Different configurations of optical arrangement as shown in Fig. 3.(a-c), were experimentally tested. Representative PPG waveforms collected from a subject consecutively for the illustrated topologies in Fig. 3.(a-c), at a sampling rate of 500 Hz are shown in Fig. 3.(e-g) respectively. The arrangement of LEDs 90° with respect to each other, with photodiode as vertex as shown in Fig. 3.(c) showed preferential results over the LEDs arranged at 180° with respect to each other as shown in Fig. 3.(a, b). Adopting the configuration shown in Fig. 3.(c) a symmetrically opposite LED is placed along the horizontal (h) axis as shown in Fig. 3.(d) to ensure a definitive contact in case of tilted motion or improper placement due to wrist bone. The configuration is aimed to maximise the area of illumination and the LEDs are positioned in a 'T'- profile on the sensor board with the photodiode on the junction of the h-axis which harbors two symmetrically positioned LEDs (LED 1 and LED 2) and the vertical (v) axis containing LED 3 as shown in Fig. 4.(a). A custom designed PCB with sufficiently long solder pads was initially used to arrive upon the optimum separation between the optical elements. This was done to ensure negligible direct optical coupling that may saturate the signal acquired by the photodetector and allow maximum admission of the reflected light containing PPG information. The PD and LEDs are aligned to the same transverse plane for escalated light admission and reception. To avoid any instance of direct coupling, appropriate optical isolators house the emitter and detector units.

In the previously developed experimental prototype presented by the authors in [11], black silicon blocks were filed and aligned adeptly to achieve the optical isolation. In the current design individual housings for each optical component are prototyped on the back side of the enclosure. The cavities are meticulously carved out to allow a perfect fit when the enclosure sits on the sensor board. In the previous design using a wired prototype presented in [11], an H-bridge configuration for LED driver circuit was used. Since

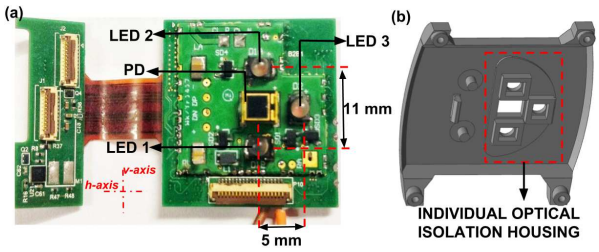

Fig. 4. (a) The optical sensor PCB illustrates the elements which are annotated as per their reference in the design. The dimensions for optimal separation is also indicated alongwith the h-axis and v-axis. (b) The back end of the enclosure casing which provides meticulously carved out cavities for the optical elements to provide absolute isolation within the components.

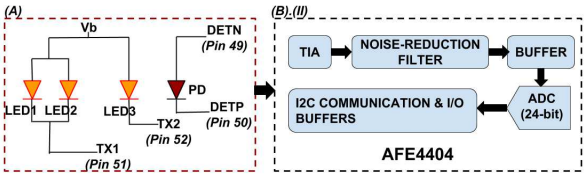

Fig. 5. Common-anode connection for the optical emitter scheme. LED1 and LED2 are parallelly connected to the first channel and LED3 is connected to the second channel. The Photodiode is connected to the front end for signal admission. The respective pins where connections are made is also annotated in the illustration.

the front end used in this device supports only a push-pull configuration, the sensor board uses a common anode mode for driving the LEDs as shown in Fig. 5. The annotations in the Fig. 5 map to the system architecture illustrated in Fig. 1. Also, Fig. 5 indicates the respective pin numbers of the front end (AFE4404, as explained later) to which the connections are made. LED 1 and LED 2 are connected in parallel to the same driving channel of the front end and LED 3 is driven by a separate channel. The exploded view of the entire design shown in Fig. 6 indicates the partitioned glass slices for the respective optical elements for isolation from skin. The backside of the enclosure exposed to the dermal surface is engraved depth-wise to enable the accommodation of this glass covering on the same plane without any additional projection or increase in the width.

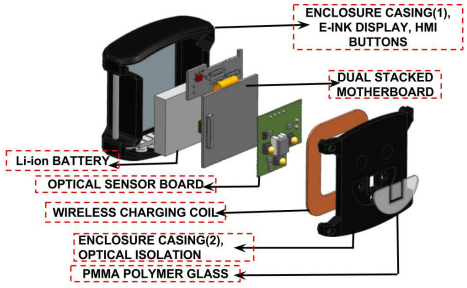

Fig. 6. Exploded view of the device showing the arrangement of all the modules.

B. Hardware Requirements of the Device and Data Acquisition

An analog front end provide by Texas Instruments, AFE4404 is used in the design. The previous wired prototype [11] used AFE4403 as the analog front end. The current choice of AFE4404 is made to achieve an improved ADC resolution of 24-bits as compared to the 22-bits. The AFE4404 communicates with the microcontroller using an I2C communication protocol. The front end can provide both raw captured signal and ambient signal. However, to economically sustain the power usage only ambient subtracted raw waveform sampled at 500 Hz is stored/streamed. The gain of the trans-impedanceamplifier (TIA) can be adjusted by manipulating the dedicated registers. AFE4404 is available in a DSBGA package of 2.6 mm $\times$ 1.6 mm. The basic modules of AFE4404 are highlighted in Fig. 5 ((B).(II)). A MEMs 3-axis accelerometer from Analog Devices Inc., (ADXL333) is integrated alongwith, to allow identification of stationary sections of the recorded data. A low-power consuming Bluetooth low energy (BLE) module of small form-factor is used in the design to stream data in real-time data for online analysis or store in a gateway device for off-line processing and analysis. The prototype is also provided with on-chip flash drive. The tear-down of the device is shown in the Fig. 6. The gateway device, is featured similar to a tablet for this prototype, however, it can be replaced by any personal computer or smartphone. The platform for waveform acquisition and off-line logging is developed using LabVIEW 2015. Fig. 7.(a) shows the optical sensor board with wireless charging coil. Fig. 7.(b) shows the backside of the wearable which is in dermal contact. Fig. 7.(c) shows a the overall measurement system with the wearable placed on the dorsal side of the non-dominant hand of the subject alongwith a gateway device. More details on teh design of the wearable are given by the authors in [15]. For the standard reference, ECG signal was acquired using eMotion Faros 360° (Mega Electronics) in single lead configuration sampled at a rate of 1000 Hz. The collected ECG and PPG signals are appropriately time synchronised prior to any processing.

IV. Algorithm Development

There are many markers used to indicate the pulse period. In the presented algorithm we use the second derivative method which allows distinctive detection of the pulse onset.

A. Pre-Processing

Use of heavy filtering techniques impact the morphology of the PPG pulse. To have minimum effect on the signal peaks and valleys a Savitzky-Golay (SG) filter of a polynomial order of 10 and window length 51 is used. This effectively corresponds to passing only components below 10 Hz.

B. Generation of acceleration plethysmograph (APG)

The first derivative of the PPG signal is called the velocity plethysmograph (VPG). This is obtained using the five-point

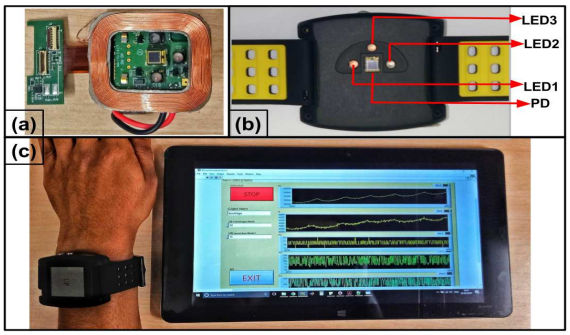

Fig. 7. (a) Designed optical sensor unit and wireless charging coil. (b) The back side of the wearable exposed to the dermal area indicating the placement and topology of the optical elements.(c) The wrist-based wearable to estimate HRV alongwith a tablet being used as the gateway device. The e-ink display can be programmed for warning or suggestive messages.

finite central difference equation as shown in Equation.1. A central difference has relatively smaller error (O(h^2)) and temporal shift (n/2) over the forward/backward difference methods. In the following instances of differentiation using numerical method the chosen step-size is $1(h = 1)$. The second derivative which is called the acceleration plethysmograph (APG), is realized using seven-point finite central difference equation as shown in Equation.2. In Equations. 1 and 2, x(n) is the current input sample from the PPG signal. The peak of the APG corresponds to the valley point of the PPG. The ideal temporal shape of the PPG signal indicates a greater slope on its onset than in its downhill path. This characteristic manifests itself as the prominent peak in the second-derivative waveform. APG improves the accuracy and ease of detection and interpretation of the inflection points. The pre-processed PPG signal, VPG and the enhanced APG (which is explained in the following section) are shown in Fig.8 (c), (d), (e) respectively.

$$V_{ppg}(n) = \frac{(x(n-2) - 8x(n-1) + 8x(n+1) - x(n+2))}{12} \quad (1)$$

$$A_{ppg}(n) = \frac{\begin{array}{c}(-x(n-3) + 9x(n-2) - 45x(n-1) \\ +45x(n+1) - 9x(n+2) + x(n+3))\end{array}}{60} \quad (2)$$

C. Feature Extraction

To emphasise and unambiguously detect the peak of APG, the value of the waveform below zero-baseline is nulled and the positive part of APG is quadrupled. This enhances the APG for peak detection. To detect these distinct peaks, blocks of interest are generated as shown in Fig.9. These blocks are generated using the idea of abrupt change in the APG waveform. The statistical metric used for quantifying this abrupt change is the mean of the current sample's neighbouring points. Once the blocks of interest are generated, the maxima in each block is denoted as the peak of APG. The peak detection of this enhanced APG is shown in Fig.8 (a), (b). The differences between the subsequent APG peaks detected correspond to PPG pulse intervals.

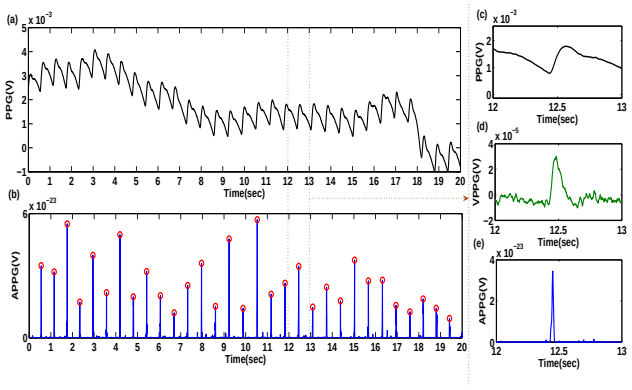

Fig. 8. (a) PPG waveform after low pass filtering (b) Emphasised APG with marked peaks (c), (d), (e) show once PPG cycle and its corresponding VPG and enhanced APG respectively.

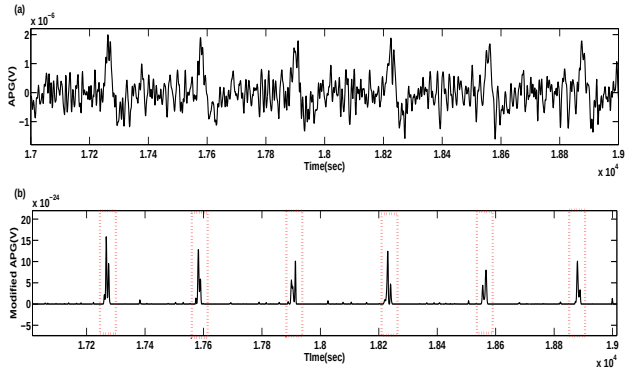

Fig. 9. (a) Generated APG from filtered PPG (b) Enhanced APG with marked blocks of interest

D. Extraction of HRV parameters

The collected ECG data is low pass filtered and using the Pan-Tompkins algorithm [16] algorithm R-peaks are detected as shown in Fig.10. A tachogram is the plot of the cardiac cycle intervals against the occurrence time. Tachogram derived from the cardiac intervals using PPG and ECG is illustrated in Fig.11 (a), (b). Before subjecting to HRV feature estimation, the tachogram is verified to eliminate any cases of outliers. Any change of subsequent intervals by more than 20% is considered an outlier and not considered in the further calculation. This 5-minute time series tachogram is used to derive the time-domain HRV features. The calculated time domain features Root Mean Square of Successive Differences (rMSSD), Standard

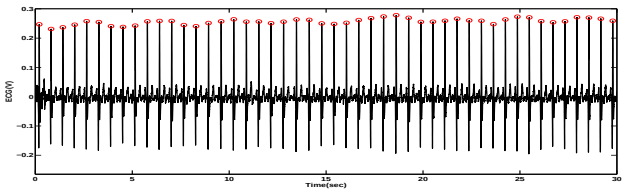

Fig. 10. ECG waveform and detected peaks using Pan-Tompkins Algorithm.

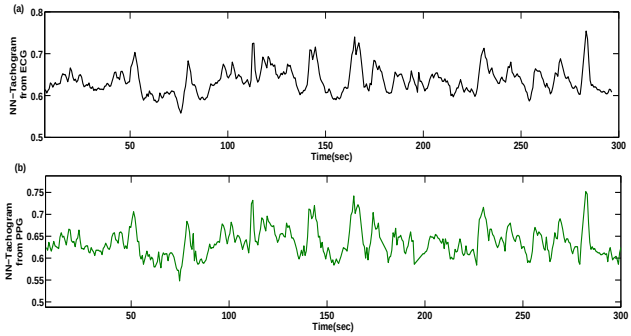

Fig. 11. (a) NN-Interval tachogram derived from ECG (b) NN-Interval tachogram derived from APG

Deviation between the NN-intervals (SDNN) and Standard Deviation of Successive Differences (SDSD) are formulated in Equation.3, 4, 5. Apart from these also another parameter which is used as a significant marker is the ratio of the number of NN-intervals (NN is a denotion for normalised intervals post outlier removal) greater than 50ms to the total number of NN-intervals. This is called as pNN50.

$$rMSSD = \sqrt{\frac{1}{P-1}\sum_{i=1}^{P-1}(NN_{i+1} - NN_{i-1})} \quad (3)$$

$$SDNN = \sqrt{\frac{\sum_i (NN_i - NN_{mean})}{P-1}} \quad (4)$$

$$SDSD = \sqrt{\frac{\sum_{i=1}^{P-1} (NN_{i+1} - NN_{i-1})}{P-1}} \quad (5)$$

V. Results and Discussions

The algorithm proposed to measure the onset of the wrist-PPG signal as the marker for a complete cardiac cycle using second-derivative method is evaluated against ECG using the following metric,

$$Sensitivity = \frac{TP}{TP + FN} \quad (6)$$

- True Positive (TP) : The peak of the APPG is correctly determined.
- False Negative (FN): The peak of the APPG is missed wrongly.

There is also a case of False Positive (FP) which refers to classifying an incorrect sample of APPG as peak.i.e. wrongly detects PPG onset. Such a case did not occur on testing the proposed algorithm on the wrist PPG waveforms. The use of block of interest eliminates such an event. These parameters were verified by keeping the ECG R-peaks as reference. However in 27 instances of the approximately 5783 cardiac cycles (sum of the detected cycles of all the 10 subjects) detected had a case of FN. This results to a sensitivity of 99.533%. A Bland-Altman plot justifying the agreement between the methods deriving the NN-interval .i.e. gold standard ECG and the wrist PPG for a subject is shown

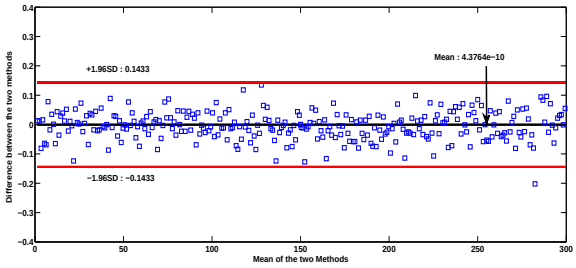

Fig. 12. Bland-Altman plot between the difference of the two methods against their mean with Lines of Agreement (LOA) specified for a 95% confidence interval (CI).

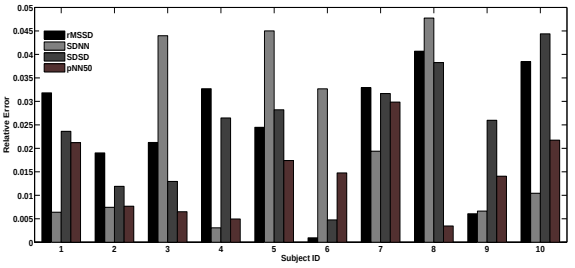

Fig. 13. Relative error between the derived time domain parameters.

in Fig.12. The limits of agreement are chosen to be 95% .i.e.±1.96SD (standard deviation). Fig.13 shows the relative errors between the parameters rMSSD, SDSD, SDNN and pNN50. Relative error is calculated as shown in Equation.7 where ECG$_{metric}$ refers to HRV features derived from ECG tachogram and same extended for the PPG$_{metric}$ also. There is no definitive trend (positive or negative bias) followed in the features. The maximum error (in all the metrics for all the subjects) is less than 5%. Using paired t-test to justify the statistically insignificant differences (α = 5%) between the two approaches we obtain p>0.005 . Also hypothesizing a null point-to-point correlation between the two methods gave p<0.0001 (favour of rejecting the null hypothesis).Using Pearson's correlation (r) to verify the temporal similarity between the tachograms for all the subjects derived from both the methods result in r>0.995.

$$RelativeError = \frac{|ECG_{metric} - PPG_{metric}|}{ECG_{metric}} \quad (7)$$

VI. Summary

HRV is an important parameter for clinical, diagnostic, physiological and psychological applications. The presented work of attempting to derive time-domain HRV features from PPG is one of a kind in its exploration of the possibility of PPG acquired from dorsal side of the wrist as the measurement site. The designed novel optical sensor provides high quality signals even at extremely low perfusion levels (due to low atmospheric oxygen content), lower temperatures till 6°C (cold ambient conditions cause microcirculation at superficial dermal levels and hinder the prominence of the cardiac palpation) and high altitudes. The agreement between the methods have been verified using bland-altman plot with 95% CI. Calculated time domain features RMSSD, SDNN, SDSD and pNN50 from PPG tachogram have relative difference less than 5%. In conclusion our results indicate that the differences between the HRV derived parameters obtained from PPG are statistically insignificant (within 95% of agreement) and wrist based PPG can be used for short term HRV monitoring. This opens up the prospect of HRV monitoring not just restricted to ambulatory events and extensively expands the serviceability of HRV.

References

[1] R. E. Kleiger, J. P. Miller, J. T. Bigger, and A. J. Moss, "Decreased heart rate variability and its association with increased mortality after acute myocardial infarction," *The American journal of cardiology*, vol. 59, no. 4, pp. 256–262, 1987.

[2] A. E. Aubert, B. Seps, and F. Beckers, "Heart rate variability in athletes," *Sports medicine*, vol. 33, no. 12, pp. 889–919, 2003.

[3] M. Horsten, M. Erigson, A. Perski, S. P. Wamala, K. Schenck-Gustafsson, and K. Orth-Gomér, "Psychosocial factors and heart rate variability in healthy women," *Psychosomatic Medicine*, vol. 61, no. 1, pp. 49–57, 1999.

[4] E. R. Migliaro, R. Canetti, P. Contreras, and M. Hakas, "Heart rate variability: Short-term studies are as useful as holter to differentiate diabetic patients from healthy subjects," *Annals of Noninvasive Electrocardiology*, vol. 8, no. 4, pp. 313–320, 2003.

[5] R. Balocchi, F. Cantini, M. Varanini, G. Raimondi, J. M. Legramante, and A. Macerata, "Revisiting the potential of time-domain indexes in short-term hrv analysis," *Biomedizinische Technik*, vol. 51, no. 4, pp. 190–193, 2006.

[6] P. Leonard, T. Beattie, P. Addison, and J. Watson, "Standard pulse oximeters can be used to monitor respiratory rate," *Emergency medicine journal*, vol. 20, no. 6, pp. 524–525, 2003.

[7] M. Nitzan, A. Babchenko, B. Khanokh, and D. Landau, "The variability of the photoplethysmographic signal-a potential method for the evaluation of the autonomic nervous system," *Physiological measurement*, vol. 19, no. 1, p. 93, 1998.

[8] F. Chang, C. Chang, C. Chiu, S. Hsu, and Y. Lin, "Variations of hrv analysis in different approaches," in *Computers in Cardiology, 2007*. IEEE, 2007, pp. 17–20.

[9] T. F. of the European Society of Cardiology *et al.*, "Heart rate variability standards of measurement, physiological interpretation, and clinical use," *Eur heart J*, vol. 17, pp. 354–381, 1996.

[10] R. Perini, S. Milesi, L. Biancardi, and A. Veicsteinas, "Effects of high altitude acclimatization on heart rate variability in resting humans," *European journal of applied physiology and occupational physiology*, vol. 73, no. 6, pp. 521–528, 1996.

[11] P. Mohapatra, S. Preejith, and M. Sivaprakasam, "A novel sensor for wrist based optical heart rate monitor," in *2017 IEEE International Instrumentation and Measurement Technology Conference (I2MTC) (I2MTC 2017)*, Torino, Italy, May 2017.

[12] R. R. Anderson and J. A. Parrish, "The optics of human skin," *Journal of investigative dermatology*, vol. 77, no. 1, pp. 13–19, 1981.

[13] J. Liu, B. P.-Y. Yan, W.-X. Dai, X.-R. Ding, Y.-T. Zhang, and N. Zhao, "Multi-wavelength photoplethysmography method for skin arterial pulse extraction," *Biomedical optics express*, vol. 7, no. 10, pp. 4313–4326, 2016.

[14] A. Bashkatov, E. Genina, V. Kochubey, and V. Tuchin, "Optical properties of human skin, subcutaneous and mucous tissues in the wavelength range from 400 to 2000 nm," *Journal of Physics D: Applied Physics*, vol. 38, no. 15, p. 2543, 2005.

[15] P. Mohapatra, P. S. Premkumar, and M. Sivaprakasam, "A yellow–orange wavelength-based short-term heart rate variability measurement scheme for wrist-based wearables," *IEEE Transactions on Instrumentation and Measurement*, vol. 67, no. 5, pp. 1091–1101, 2018.

[16] J. Pan and W. J. Tompkins, "A real-time qrs detection algorithm," *IEEE transactions on biomedical engineering*, no. 3, pp. 230–236, 1985.